Effect of Neutron Irradiation on the Structural, Mechanical, and Thermal Properties of Jute Fiber

E. Sinha,[1] S. K. Rout[2]

[1]*Department of Physics, National Institute of Technology, Rourkela 769008, Orissa, India*
[2]*Department of Applied Physics, Birla Institute of Technology, Mesra, Ranchi, Jharkhand, India*

Received 20 April 2007; accepted 30 March 2008
DOI 10.1002/app.28504
Published online 9 July 2008 in Wiley InterScience (www.interscience.wiley.com).

ABSTRACT: This article describes the effect of neutron irradiation on jute fiber (*Corchorus olitorius*). The jute fibers (4.0 tex) were irradiated by fast neutrons with an energy of 4.44 MeV at different fluences ranging from 2×10^9 to 2×10^{13} n/cm^2. An important aspect of neutron irradiation is that the fast neutrons can produce dense ionization at deep levels in the materials. Structural analysis of the raw and irradiated fibers were studied by small-angle X-ray scattering (SAXS), X-ray diffraction (XRD), scanning electron microscopy (SEM), and Fourier transform infrared spectroscopy. Thermal analysis carried out on the raw and irradiated fibers showed that the thermal stability of the fibers decreased after irradiation. The mechanical properties of the jute fibers were found to decrease after irradiation. The SAXS study showed that the average periodicity transverse to the layer decreased after irradiation, which may have been due to the shrinkage of cellulosic particles constituting the fiber. The residual compressive stress developed in the fiber after irradiation resulted in a decrease in crystallite size as supported by our XRD analysis. Observation with SEM did not indicate any change produced in the surface morphology of the fiber due to irradiation. © 2008 Wiley Periodicals, Inc. J Appl Polym Sci 110: 413–423, 2008

Key words: differential scanning calorimetry (DSC); fibers; mechanical properties; SAXS; X-ray

INTRODUCTION

Mounting concerns for the environment have sparked renewed interest in the development of biodegradable, mechanically sound alternatives to plastics through the use of natural fibers.[1] Natural fibers can be used as reinforcement in a degradable polymer matrix and, thus, serve as inexpensive, biodegradable, renewable, and nontoxic alternatives to glass or carbon fibers and offer high specific properties such as strength and stiffness.[1] The main limitations of these fibers are their hydrophilic nature, low thermal resistance, and quality inconsistencies.[2] The surface treatment of fibers is mainly used to improve their properties and is, therefore, widely applied to natural fibers.[3] The influence of radiation on synthetic and natural polymers has been studied quite extensively over the last few decades.[4,5] Jute fiber is a natural polymer, composed[6] mainly of cellulose (58–65%), hemicelluloses (20–22%), and lignin (12–15%). It is widely used in the textile industry, diversified applications in engineering, and where light weight is required, such as for building materials and structural parts for automotive applications. However, if the desired properties of jute fiber could be improved by neutron-irradiation-induced physical modification, value-added products could be made from such materials.

The effect of fast neutron irradiation on polymer seems interesting from both the basic and practical point of view. Fast neutrons irradiated on organic materials interact mostly with protons of the materials and produce recoil protons of high energy as a result of inelastic collisions. Therefore, the chemical effect of the fast neutron is considered to be equal to that of high-energy protons.[7] Many researchers have worked on the effects of neutron irradiation on synthetic fibers,[8–10] but much less is found in the field of natural fibers.

As jute fiber is cellulosic in nature and comes under a macromolecular system, we used small-angle X-ray scattering (SAXS) to analyze some of its macromolecular structural parameters. To be specific, SAXS is due to the heterogeneity of electron density occurring in matter at colloidal dimensions. When matter contains various homogeneous regions in its interior with various electron densities, SAXS takes place because of the variation of electron density over a distance of the order of 10 to 1000s of angstroms. There will be no scattering if the density is uniform. For the sake of demonstration, our system was considered a two-phase (cellulose and void) one, and the square of electron density difference took about 100 times the value of that between the crystalline and amorphous celluloses. Hence, we treated jute as a two-phase system with the cellulose and the void as its two phases. This phenomenon

Correspondence to: E. Sinha (elasinha@rediffmail.com).

was first observed by Krishnamurti,[11] Mark,[12] and Hendricks[13] around 1930. Porod's laws[14,15] were applied to obtain the physical parameters of the densely packed system for an ideal two-phase structure having sharply defined phase boundaries. Later, Vonk[16] explained that the electron density does not change abruptly but changes gradually over a certain range between the two phases. This range is called the *width of the transition layer* (*E*). Such a system is known as a *nonideal two-phase system*. This model of a nonideal two-phase system can be considered as one in which the hard core is coated with a soft sheath with a continuously varying electron density. In this investigation, an effort was made to study some of the mechanical and thermal behaviors of raw (dewaxed) and fast neutron-irradiated jute fibers with fluences of 2×10^9, 2×10^{11}, and 2×10^{13} n/cm^2. We tried to correlate this behavior with the macromolecular structure by SAXS at room temperature. The crystallinity and surface morphology were investigated by X-ray diffraction (XRD) and scanning electron microscopy (SEM) methods. Fourier transform infrared (FTIR) spectra were recorded to study the fine structural characteristics of the cellulose, hemicelluloses, and lignin. Thermal properties were analyzed by differential scanning calorimetry (DSC) of the raw and irradiated jute fibers.

EXPERIMENTAL AND CORE MATHEMATICS

Materials

Jute fibers (*Corchorus olitorius*) were collected from the Central Research Institute for Jute and Allied Fiber Technology (Kolkata, India).

Methods

Dewaxing

Collected fibers were dewaxed in a 1 : 2 mixture of alcohol and benzene as done by Roy.[17] As a result of this treatment, the specimen attained a "hohlraum" character (according to Porod[18] and Ratho and Sahu[19]); that is, the substance occurred in layers like the pages of the book with free space in between. This was treated as the raw sample in this study.

Neutron irradiation

The radioactive neutron source[20] used in laboratories is mainly based on either spontaneous fission or nuclear reactions. The latter is a more convenient method for producing neutrons. Nuclear reactions of α, η and η, γ types occur with many nuclei with the excited energy greater than the neutron binding energy, which can decay, to neutron emission; however, only those with the highest yield are used. Generally, such sources are made by the mixture of the target material, such as beryllium, with a suitably strong α or γ emitter. When bombarded by α particles, beryllium undergoes a number of reactions that lead to the production of free neutrons[21] as follows:

$$ {}^4_2\alpha + {}^9_4\mathrm{Be} \rightarrow {}^{13}\mathrm{C}^* \rightarrow \begin{cases} {}^{12}\mathrm{C} + {}^1_0\eta \\ {}^8_4\mathrm{Be} + {}^4_2\alpha + {}^1_0\eta \\ 3{}^4_2\alpha + {}^1_0\eta \end{cases} $$

where ^{13}C* is the excited compound nucleus formed, which decays through a variety of ways, depending on the excited energy. The dominant reaction, however, is the decay to ^{12}C or to the 4.44-MeV excited state of ^{12}C. The neutron radiation source used for this irradiation study was produced from an Am-Be source by an α, η type nuclear reaction. With Am^{241} taken as a α source of energy (5.48 MeV), an experimental neutron yield of about 70 neutrons per 10^6 α's is generally obtained from a beryllium target. A neutron beam with an energy of 4.44MeV and a flux of 2.2×10^6 n cm^{-2} s^{-1} was used to irradiate samples in air at atmospheric pressure in the temperature range 22–27°C for different exposure times to get three different fluences: 2×10^9, 2×10^{11}, and 2×10^{13} n/cm^2; these samples are referred to as neutrons 1, 2, and 3, respectively, hereafter.

SEM study

Scanning electron micrographs of the samples were taken in a Hitachi (S-3400N) [USA] scanning electron microscope. The samples were coated with a 20 nm thick gold layer.

FTIR spectroscopy

The raw and neutron-irradiated jute fibers were analyzed by FTIR spectroscopy. Room-temperature FTIR spectra were recorded on solid samples in KBr pellets by means of a Shimadzu FTIR (Shimadzu, Japan) spectrometer (IRPrestige-21) with a resolution of 4 cm^{-1}. The spectrums were smoothed with a constant smooth factor for comparison.

SAXS

X-ray measurement and computational analysis. Room-temperature smeared-out SAXS data for the jute fibers were collected form a line collimated SAXSess camera (Anton Park, Austria). The Cu Kα lines were used as incident radiation from a PANalitica X-ray source (PW3830) [Philips, Netherland] at an operating voltage of 40 kV (40 mA). The sample-to-detector distance was 26.45 cm. The scattering intensities were collected in a two-dimensional position sensitive image plate (Packard Bioscience, Inc.) [USA]. To obtain digitized data, the image plate was scanned in a cyclone storage phosphor scanner (PerkinElmer)

[Waltham, USA] with the help of the supplied computer program Optiquant. The observed two-dimensional intensities were integrated over a line profile to convert into one-dimensional scattering data with the help of the supplied computer program SAXS Quant. All of the computations were performed with a self-developed program written in MATLAB 6.5 (the Mathworks, Inc., Natick, USA). The program comprised the computation of the relevant parameters by SAXS, including one- and three-dimensional correlation functions. The reliability of the program was checked with the experimental data and the results for sisal fiber, which is available from the authors.

Theory. It was shown by Vonk[16] that for a general two-phase system having an isotropic structure, the following relation holds good:

$$16\pi^3 \int_0^\infty s^4 I_a(s)ds = \int_0^\infty \left|\text{grad } \eta\right|^2 dV_r \quad (1)$$

V_r is total volume of the particle where $I_a(s)$ is the desmeared intensity in the absolute units, η is the deviation of the electron density of the sample at any point from the mean value, and s is the coordinate in the reciprocal or Fourier space given by the relation $s = 2\theta/\lambda$ (wavelength of incident radiation), where 2θ is the scattering angle and is equal to x/a, where x is the position coordinate of the scattered intensity from the center of the primary beam. The previous equation can be regarded as parallel to the well-known relation

$$4\pi \int_0^\infty s^2 I_a(s)ds = \int_0^\infty \eta^2 dV_r \quad (2)$$

where $\int_0^\infty s^2 I_a(s)ds$ is generally known as the invariant.

If the absolute intensities are not available, a very useful parameter (R), given by the ratio of eqs. (1) and (2), can be obtained as

$$R = \frac{\left|\text{grad } \eta\right|^2}{\eta^2} = 4\pi^2 \int_0^\infty s^4 I_a(s)ds \Big/ \int_0^\infty s^2 I_a(s)ds = 6\pi^2 \int_0^\infty s^3 \tilde{I}(s)ds \Big/ \int_0^\infty s\tilde{I}(s)ds\tilde{I} \quad (3)$$

where $\tilde{I}(s)$ is the smeared-out intensity in arbitrary units.

The ratio R is a useful parameter for the characterization of the structure. In any ideal two-phase structure, the gradient at the phase boundary is infinite, and consequently, R also goes to infinity. On the other hand, if R is finite and varies continuously over the region known as the width of the transition layer or layer thickness (E), the previous equation is transformed to variable x, by Misra et al.,[22] as

$$R = (3/2)(2\pi/\lambda a)^2 \int x^3 \tilde{I}(x)dx \Big/ \int x\tilde{I}(x)dx = (3/2)K^2 A_3/A_1 \quad (4)$$

$$K = 2\pi/(\lambda a),\ A_3 = \int x^3 \tilde{I}(x)dx \text{ and } A_1 = \int x^3 \tilde{I}(x)dx\,.$$

The value of R obtained from eq. (4) determines the nature of the samples, as to whether they belong to an ideal or nonideal two-phase system.

In the case of a nonideal two-phase system, the important parameter is the width of the transition layer (E). The value of E can be obtained from the three-dimensional correlation function of a sample normalized to unity at the origin in real space [$C(r)$]. The equation connecting E and $C(r)$ was given by Vonk[16] as

$$E_v = -4/R_1 (dC(r)/dr)_{r=E_v} \quad (5)$$

To obtain E, one must evaluate the value of $C(r)$ at various values of r in real space. It has been shown by Mering and Tchoubar[23] that $C(r)$ can be calculated from the expression

$$C(r) = \int_0^\infty s\tilde{I}(s)J_0(2\pi rs)ds \Big/ \int_0^\infty s\tilde{I}(s)ds \quad (6)$$

where the J_0 is the Bessel function of the zero-order first kind. In the previous expression, $C(r)$ is determined from $\tilde{I}(s)$, where the slit correction for infinite height given by the relation, $\tilde{I} = \int_{-\infty}^{\infty} I\left(\sqrt{s^2 + t^2}\right)dt$ is incorporated[24] and contained in J_0. Here, t is the arbitrary variable representing the slit height and $C(r)$ is written in terms of x, by Misra et al.,[22] and is given by

$$C(r) = \int_0^\infty x\tilde{I}(x)J_0\left(\frac{2\pi rx}{\lambda a}\right)dx \Big/ \int_0^\infty x\tilde{I}(x)dx \quad (7)$$

For a layer structure, Kortleve and Vonk[25] used the one-dimensional correlation function [$C_1(y)$]. Mering and Tchoubar[26] showed that

$$C_1(y) = \int_0^\infty sI(s)[J_0(Z) - ZJ_1(Z)]ds \Big/ \int_0^\infty sI(s)ds \quad (8)$$

where $Z = 2\pi sy$ and J_1 is the Bessel function of the first-order first kind. When changed to the x variable, the previous equation (Misra et al.[22]) reduces to

$$C_1(y) = \int_0^\infty x\tilde{I}(x)[J_0(Z) - ZJ_1(Z)]dx \Big/ \int_0^\infty x\tilde{I}(x)dx \quad (9)$$

where $Z = 2\pi sy/\lambda a$. Vonk[16] showed that the position of the first very maximum in $C_1(y)$ gives the value of the average periodicity transverse to the layers (D). The value of D can be obtained by picking up the position of the first subsidiary maximum in the $C_1(y)$ versus y (points for which one-dimensional correlation function were computed) curve.

The equation

$$(dC_1(y)/dy)_{y>E_v} = -1(\Delta\eta)^2/D\langle\eta^2\rangle \quad (10)$$

derived by Vonk[16] can be used to calculate the value of $(\Delta\eta)^2/\langle\eta^2\rangle$, where $\Delta\eta$ is the electron density difference between the two phases. Here, the slope is taken at a point where y is greater than E_v. It was also proved by Vonk[16] that the second differentials of $C(r)$ and $C_1(y)$ at the origin is given by the relation

$$\left(d^2C_1(y)/dy^2\right)_{y=0} = 3\left(d^2C(r)/dr^2\right)_{r=0} \quad (11)$$

For a layer structure, as shown by Vonk,[16] the *specific inner surface* (S/V) is defined as the phase boundary per unit volume of the dispersed phase and can be written as

$$S/V = 2/D \quad (12)$$

For a nonideal two-phase structure, the following relation holds good:[16]

$$\langle\eta^2\rangle/(\Delta\eta)^2 = \phi_1\phi_2 - (ES/6V) \quad (13)$$

where ϕ_1 and ϕ_2 are the volume fractions of the matter and void regions, respectively. For this, the phase boundary is shown at the middle of the transition layer. If the sum of the volume fraction of both phases is assumed to be the unit, the values of ϕ_1 and ϕ_2 can be determined from the previous relation.

For the two-phase structure, one can form an idea of the statistical distribution of the crystalline (matter) and void regions by shooting arrows in all of the possible directions. The average lengths of the arrow in the matter and in the void are called the *transversal lengths* [$\bar{l}_1$ and $\bar{l}_2$, respectively]. They were given by Mittelbach and Porod[26] as

$$\bar{l}_1 = 4\phi_1 V/S \qquad \bar{l}_2 = 4\phi_2 V/S \quad (14)$$

with the range of inhomogeneity [$\bar{l}_r$] as

$$1/\bar{l}_r = 1/\bar{l}_1 + 1/\bar{l}_2 \quad (15)$$

The length of the coherence (l_c) for a specimen as given by previous worker is

$$l_c = 2\int_0^\infty C(r)dr \quad (16)$$

The value of E can also be calculated by the Ruland method[27] from the plot of (smeared-out SAXS intensities) $\tilde{I}(x)(x)$ versus x^{-2}, known as a *Ruland plot*. The functional relationship of $\tilde{I}(s)$ with s at the tail end of the SAXS pattern for a nonideal two-phase system is given by

$$\tilde{I}(s \to \infty) = \pi c/2(1/s^3 - 2\pi^2E^2/3s) \quad (17)$$

where c is the proportionality constant. For an ideal two-phase structure, $E = 0$, and hence, the previous equation reduces to Porod's law. The previous equation, when transformed to x, takes the form

$$\tilde{I}(x \to \infty)x = \pi c/2(x^{-2} - \pi^3 c/3(\lambda a))E^2 \quad (18)$$

The value of E can be calculated from the graph of $\tilde{I}(x \to \infty)x$ versus x^{-2}, known as a Ruland plot.

Background correction. In no experimental set up is it possible to record the SAXS pattern of the sample alone. A continuous background scattering is always mixed with the SAXS pattern of the experimental sample. It is, therefore, essential to apply the background correction to estimate the effect of continuous background scattering. Therefore, special care must be taken to separate the SAXS intensity [$\tilde{I}(s)$] from the continuous background scattering [$\tilde{I}_{bg}$ (a smeared-out background SAXS intensities) (s)] as shown by Vonk[16].

XRD

Experimental techniques. The XRD [Netherland] data were collected with a Philips Analytical x-ray instrument (X'Pert-MPD, PW 3020 vertical goniometer, and 3710 MPD control unit) [Netherland] with Bragg–Brentano parafocusing optics. The XRD patterns were recorded with a step size of 0.01° on a 5–50° range with a scanning rate of 2°/min. Line-focus Ni-filtered Cu Kα radiation from an X-ray tube (operated at 40 kV and 30 mA) was collimated through a soller slit of 0.04 rad, a fixed divergence slit of 1°, and a mask (5 mm) before it was diffracted from the sample. Experimental control and data acquisition were fully automated through a computer.

Principle. The strains developed in crystallites due to radiation heating or irradiation manifest as change in the lattice planes, which causes line shifting.

These changes in the lattice planes were measured by the XRD method. Microstress causes diffraction line broadening, whereas macrostress causes line shifting. The relation between the broadening produced and the nonuniformity of the strain can given by the formula $b = \Delta 2\theta = -2\Delta d \tan \theta/d$, derived by differentiation of Bragg's law, where b is the extra broadening, over and above the instrumental breadth of the line due to a fractional variation in plane spacing $[\Delta d/d]$ to be calculated from the observed broadening.

If d_u indicates the nonirradiated (unstressed) spacing and d_s is the spacing in the irradiated (strained) fiber, the microstrain in the particles in the direction normal to the diffracting plane (ε) is

$$\varepsilon = \Delta d/d = \left(d_s - d_u/d_u\right) \tag{19}$$

If $d_s > d_u$, $\Delta d/d$ is positive, which indicates that the residual stress is tensile, and if $d_s < d_u$, $\Delta d/d$ is negative, which indicates the generation of residual compressive stress in the surface. This value of $\Delta d/d$, however, includes both tensile and compressive strains. Assuming both are equal for microcrystallites, the value of $\Delta d/d$ must be divided by two to obtain the maximum tensile strain alone or the maximum compressive strain alone.[28] Again, the maximum microstress present in a sample (σ_{stress}) can be defined as

$$\sigma_{stress} = \varepsilon E/2 \tag{20}$$

Putting the value of the ε, we obtain

$$\sigma_{stress} = \Delta d E/2d \tag{21}$$

where E is the elastic constant, generally known as the Young's modulus of the material.

The crystallite size of the samples was calculated with the well-known Scherrer formula.[28] The crystallinity index (CrI) of the fibers was calculated according to the Segal empirical method.[29]

Mechanical property analysis

Tensile tests of single jute fibers were carried out with an Instron 1185 at the National Institute of Research on Jute and Allied Fiber Technology (Kolkata, India). A gauge length of 10 mm was used with a crosshead speed of 5 mm/min. Fifty fibers of both irradiated and untreated samples with a length 50 mm and a magnification of 50 : 1 were tested, and the mean values were considered.

Thermal analysis

DSC measurements were performed with a TA Instruments model Q 10 thermal analyzer (TA instruments, UK, model Q 10). A heating rate of 10°C/min and a sample weight of 3–4 mg in an aluminum crucible with a pin hole were used in a nitrogen atmosphere (50 mL/min).

RESULTS AND DISCUSSION

Surface morphology by SEM

The surface morphologies of the raw and neutron-irradiated jute fibers were analyzed by SEM. The SEM pictures of both the raw and irradiated jute fibers are shown in Figure 1. The surface of the jute fibers was found to be smooth and multicellular in nature before and after irradiation. However, defects on the surfaces of the fibers could be seen after irradiation.

FTIR study

Figure 2 shows the spectra of the raw and fast neutron-irradiated jute fibers. The strong absorption between 3400 and 3600 cm^{-1} in all of the FTIR spectra was caused by the OH groups of the fiber constituents.[30] The strong absorption near 2925 cm^{-1} in all of the spectra was due to the strong aliphatic C—H stretch, which was due to the alkane residues contained in the organic compounds. The irradiated jute fiber led to an increase in the absorption in the regions 1735–1737 cm^{-1}, which was assigned to C—O stretching of the carbonyl and acetyl groups in hemicellulose. This improvement in the peak absorption after neutron irradiation was perhaps due to the esterification of the hydroxyl group, which resulted in increased stretching vibrations of the carbonyl (C=O) group present in the ester bonds. The absorption band found with equal intensity between 1650 and 1590 cm^{-1} in all of the FTIR spectra was mainly due to the N—H bending vibration of the primary amines present in the hemicelluloses. The absorption peaks at about 1450 and 1370 cm^{-1} found in all of the spectra were due to the bending vibrations of methylene groups presents in lignin and C—H; deformation may have been due to lignin, cellulose, or xylan. The absorption between 1250 and 1020 cm^{-1} was due to C—N stretching vibrations of the unconjugated C—N linkages in amines, which did not change their positions or relative intensities in any of the spectra.

Macromolecular structure of the fibers

The experimental SAXS patterns for the raw and fast-neutron-irradiated jute fibers at room temperature attained a minimum and stable value at $x \geq 4$ mm. Hence, the intensity at $x = 4$ mm was treated as the background scattering intensity; it was subtracted from the observed intensity and plotted in Figure 3. The background-corrected SAXS intensities

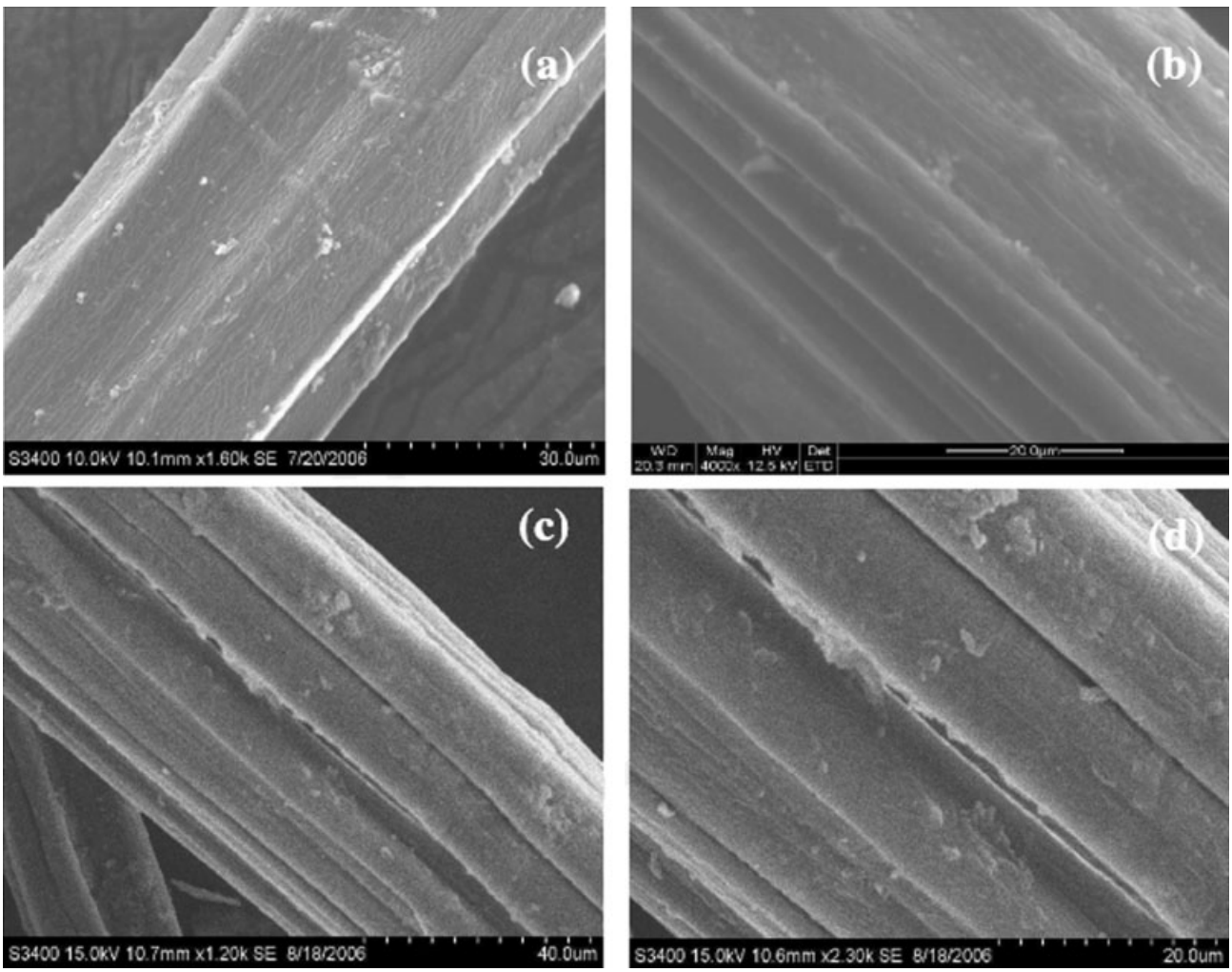

Figure 1 Surface morphology of different jute fibers: (a) raw jute, (b) neutron 1, (c) neutron 2, and (d) neutron 3.

were used for subsequent calculation and plots. At the outset, five background-corrected intensity values near the origin were fitted to a Gauss curve[31] $[\tilde{I}(x \rightarrow 0) = p \exp(-qx^2)]$ by the least squares technique. The values of the constants p and q were obtained as 191.4 and 419.9 for the raw jute, whereas

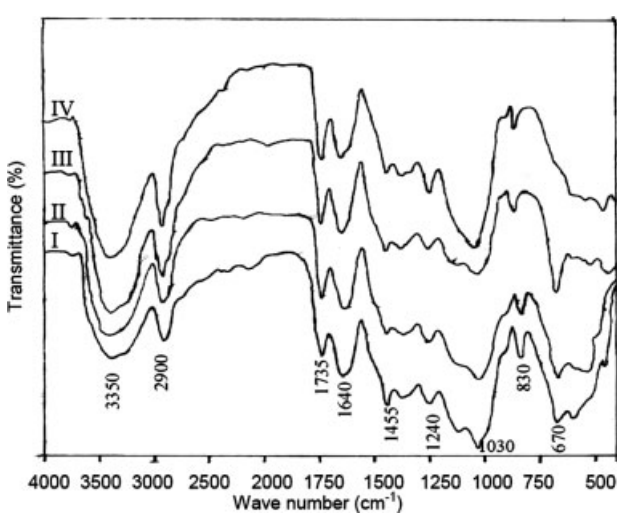

Figure 2 Infrared spectra of the raw and neutron-irradiated jute fibers.

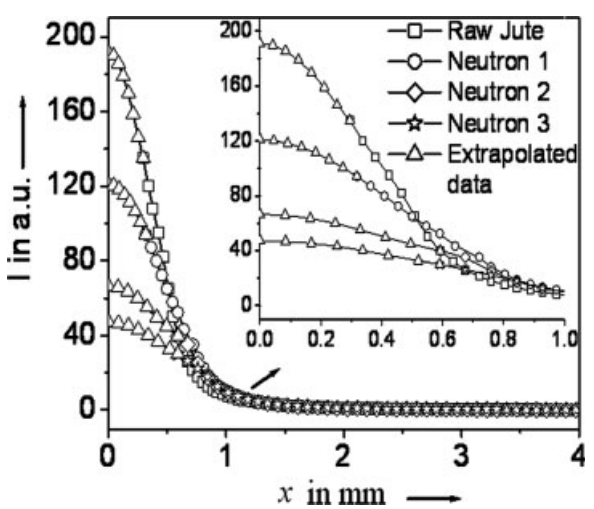

Figure 3 Background-corrected, smeared-out scattering curves for different jute fibers.

TABLE I
Various Physical Parameters of the Raw and Neutron-Irradiated Jute Fiber Derived from the SAXS Study

Parameter (unit)	Sample			
	Raw jute	Neutron 1	Neutron 2	Neutron 3
R (10^{-2} nm^{-2})	3.05	3.09	3.94	4.47
D (nm)	85.0	60.0	55.0	50.0
E_v (nm)	4.75	5.20	4.90	4.80
E_R (nm)	4.55	4.90	5.10	5.0
ϕ_1 (%)	0.806	0.733	0.696	0.632
ϕ_2 (%)	0.194	0.266	0.304	0.368
S/V (10^{-2} nm^{-1})	2.35	3.33	3.63	4.0
$\bar{l}_1$ (nm)	137.11	88.14	76.74	63.16
$\bar{l}_2$ (nm)	32.8	33.0	33.25	36.83
$\bar{l}_r$ (nm)	26.52	23.40	23.20	23.26
l_c (nm)	38.78	32.35	27.29	24.46
σ	0.03	0.007	0.03	0.013

p and q values of 121.42 and 249.98 were obtained for neutron 1, 66.9 and 174.87 were obtained for neutron 2, and 47.38 and 148.15 were obtained for neutron 3, respectively. With the values of p and q, the scattering curve for all of the cases were extrapolated to $x = 0$. Each extrapolated point is indicated by the symbol $\triangle$ in Figure 3. The method of extrapolation had little effect on the relevant part of the correlation function; neither the position nor the height of the first maximum of $C_1(y)$ was affected. The two integrals in eq. (4) were calculated by numerical integration with the trapezoidal rule, and the value of the R was found to be positive for all of the samples, as shown in Table I. The small but positive value of R indicated that the electron density gradient at the phase boundary was finite, which suggested the sample to be a nonideal two-phase system.[31]

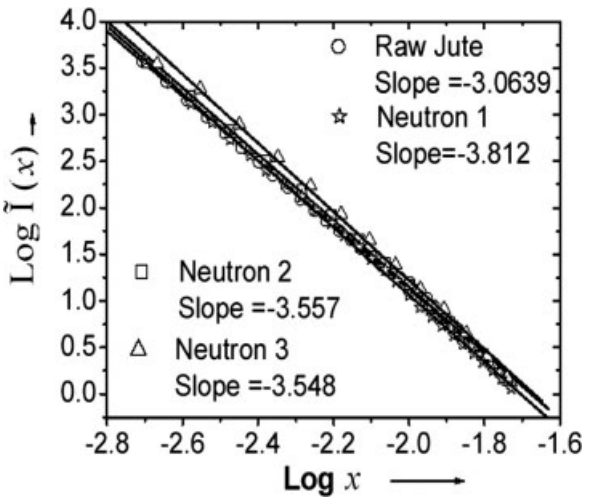

Figure 4 Double logarithmic plot of the background-corrected, smeared-out scattering curves for different jute fibers.

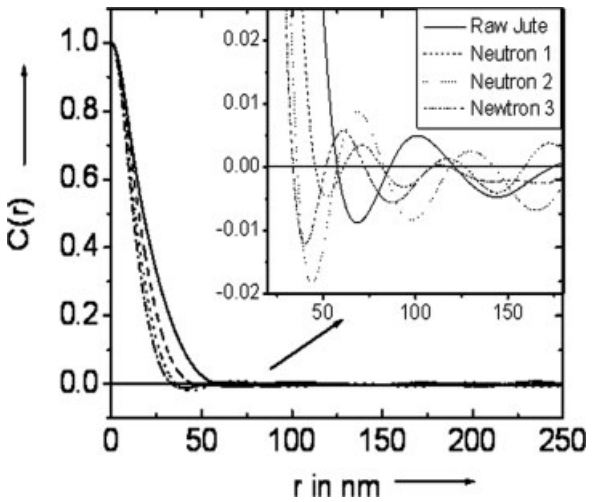

Figure 5 Curves showing $C(r)$ against r values for raw jute, neutron 1, neutron 2, and neutron 3.

After proper background correction, to have a clear idea of the samples, a double logarithmic plot was used and is shown in Figure 4. The slope of each plot is given in the legend for each sample. For the various values of r and y, the three-dimensional correlation function and $C_1(y)$ for the samples were computed and are shown in Figures 5 and 6, respectively. It has been reported[32,33] that cellulose has a layer structure. Therefore, we assumed that the cellulose fibrils in the jute fibers were arranged in layers to give a lamellar structure. That is why $C_1(y)$ was applied and calculated for all of the jute fiber samples. According to Vonk, the width of the transition layer (E_v) was obtained from the plot of $-\{4/R[dC(r)/dr]\}$ versus r, as shown in Figure 7. The value of D were obtained from the position of the first subsidiary maxima in $C_1(y)$ (Fig. 7). The value of S/V, ϕ_1 and ϕ_2, $\bar{l}_1$ and $\bar{l}_2$, $\bar{l}_r$, and l_c were estimated. All main

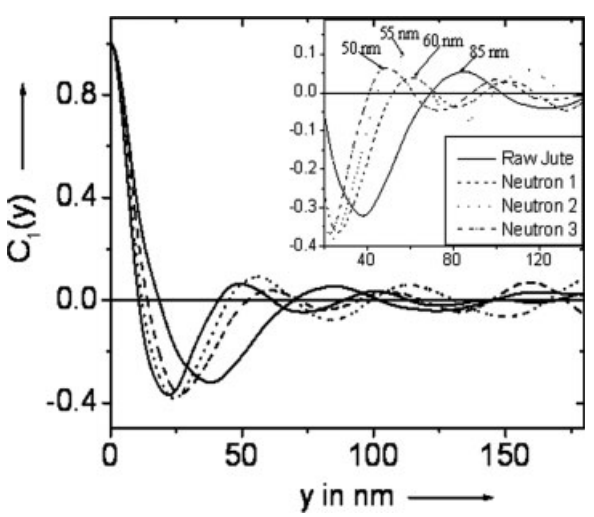

Figure 6 Curves showing the values of $C_1(y)$ against y values for raw jute, neutron 1, neutron 2, and neutron 3.

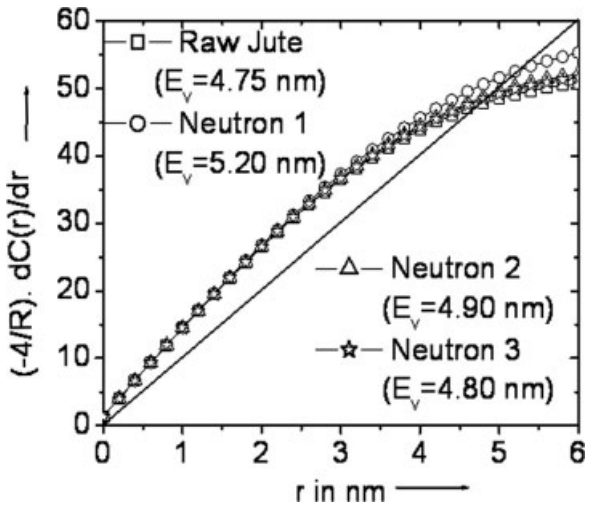

Figure 7 Curves showing the value of $(-4/R)dC(r)/dr$ against r values for different jute fibers. The values of E_v for the representative fibers are given in parentheses.

SAXS parameters are shown in Table I. All the tabulated data were consistent with those observed for other natural fibers, such as cotton[34] and sisal.[35] The width of the transition layer could also be calculated with Ruland's method. The plot of x^{-2} versus $\tilde{I}(x)(x)$ is popularly known as Ruland's plot. The Ruland's plots were plotted with background-corrected intensity values of 40 and are shown in Figure 8. Straight lines were fitted with 15 extreme points of the tail region of the corresponding scattering curve. The negative intercept of the regression line confirmed the nonideal, two-phase system.

The values of the width of the transition layer determined by the Ruland method (E_R)[21] were computed for each sample by substitution of the values of slope m and y intercept (b) of the line in the relation $E_R = [(-6b/m)^{1/2}]/(2\pi/\lambda a)$ and are shown in Table I. The standard deviation of the intensities $[\sigma(\sqrt{\tilde{I}})]$ was calculated at the tail region of the SAXS curve of the samples, and the values were well within permissible limits (0.5; Table I).[31] The lamellar model based on the previous findings is shown in Figure 9.

Table I shows that D increased in the neutron-irradiated fibers in comparison to the raw jute fibers. Similarly, the values of ϕ_1 and $\bar{l}_1$ were found to decrease after irradiation. This suggested that the shrinkage of cellulosic particles constituting the fibers may have been due to chain scissoring after irradiation. The values of E, the width of the transition layer, calculated by two different methods, that is, by the Vonk[16] method and the Ruland[27] plot method, referred as E_v and E_R, respectively, were in the permissible range of deviation. $\bar{l}_r$, which has the

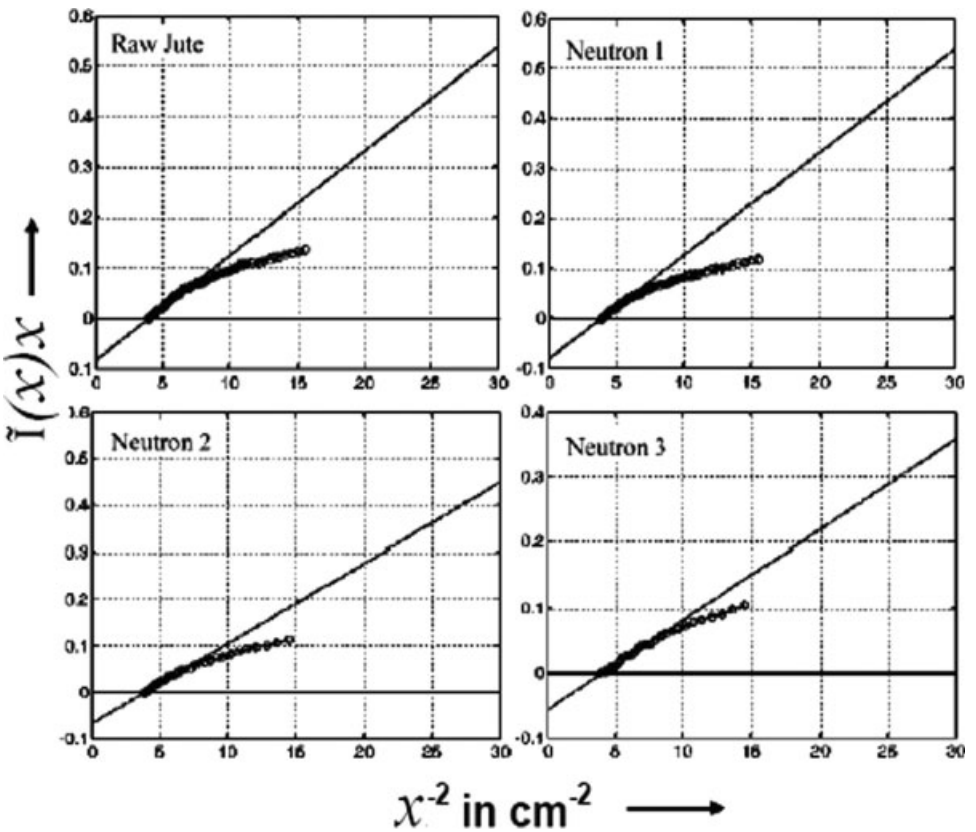

Figure 8 Ruland plot of $\tilde{I}(x)x$ versus x^{-2} for (a) raw jute, (b) neutron 1, (c) neutron 2, and (d) neutron 3.

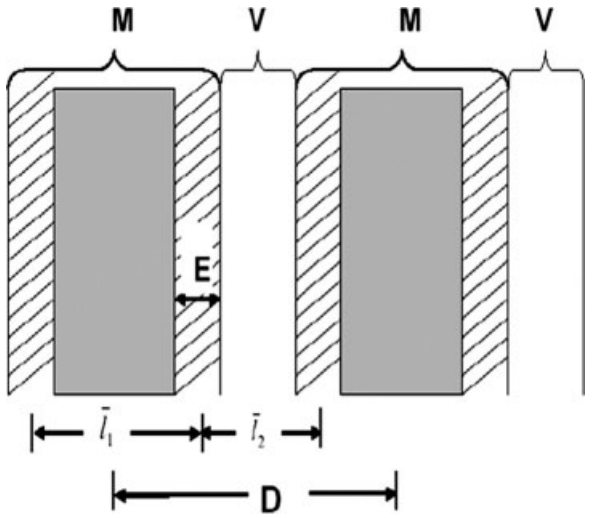

Figure 9 Lamellar model (not to scale) for different jute fibers (M = matter; V = void; E = width of the transition layer).

same meaning of reduced mass in mechanics, decreased after irradiation, which led to a decrease in the disorderliness of the system.

XRD analysis

Figure 10 shows the room-temperature XRD pattern of the jute fiber samples before and after irradiation with 4.44-MeV neutrons at different fluences. The pattern shows that the 002 peak shifted slightly toward a higher angle, which indicates a decrease in d spacing. The microstress and percentage crystallinity were also calculated from the diffractogram and are presented in Table II. From the table, it is clear that the full width at half-maximum of the diffraction peak increased and that compressive stress developed in the fiber after irradiation. However, the crystallite sizes and CrI, measured by the Segal empirical method, showed little change in the raw and irradiated fibers. Similar results have also been observed by other research groups working on natural fibers.[30,36,37]

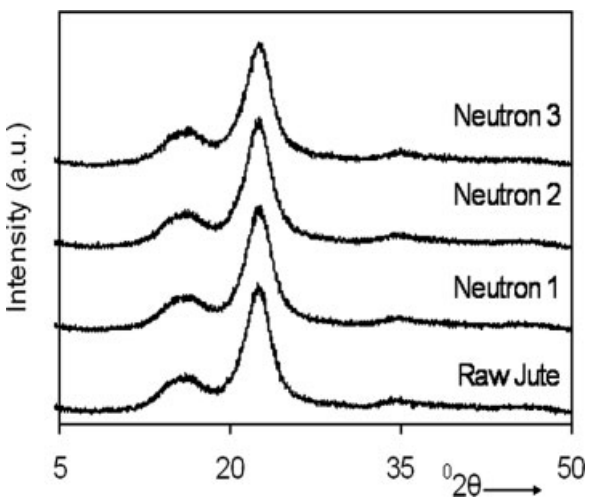

Figure 10 XRD patterns of the jute fiber samples before and after irradiation with 4.44-MeV neutrons at different fluences.

TABLE II
Observed and Calculated Parameters from the XRD Patterns

Parameter	Sample			
	Raw jute	Neutron 1	Neutron 2	Neutron 3
Irradiation fluences (n/cm^2)	0	2×10^9	2×10^{11}	2×10^{13}
Peak position (2θ)	22.5	22.51	22.55	22.56
FWHM (2θ)	2.772	2.795	2.847	2.884
d (nm)	0.394	0.394	0.392	0.391
Crystallite size (nm)	29	28	28	28
ε	0	0.0004	0.0024	0.0029
I_{002} (counts/s)	1664	1638	1651	1677
I_{am} (counts/s)	569	571	578	591
CrI (%)	65.80	65.12	64.98	64.75
σ_{stress} (10^{-4} N/tex)	0	0.219	1.315	1.589

I_{002} and I_{am} is intensities peak due to crystalline and amorphous region of the fibre respectively.

Mechanical properties

Figure 11 shows the variation of linear density (tex) of the fibers with neutron fluences of 2×10^{13} n/cm^2 or less. The figure shows a decreasing trend of the tex with treatment time. In this case, the linear densities of the fibers decreased from 4 to 2.7 tex for the raw jute to the highest neutron fluences of 2×10^{13} n/cm^2.

Figure 12 shows the change in strain at break point, tenacity, and modulus of the fibers due to

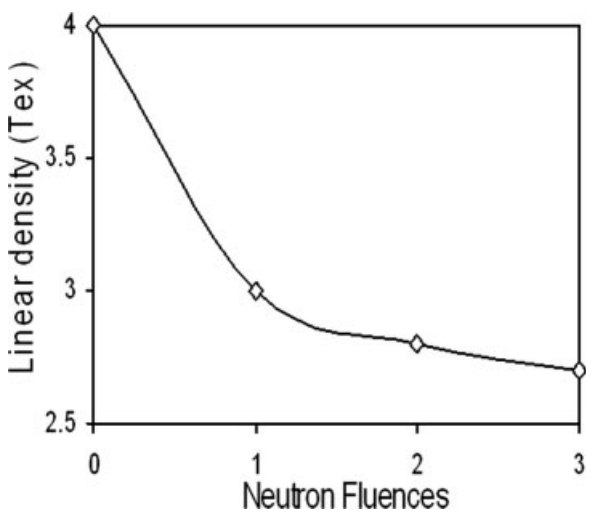

Figure 11 Variation of the linear density with different neutron fluences.

irradiation. As shown in the figure, the strain at break point, tenacity, and Young's modulus of the fibers decreased as the neutron fluences increased. This may have been due to the residual compressive stress developed in the fiber, which led to a decrease in the size of the fiber crystallite, as supported by our XRD analysis.

Thermal analysis

DSC analysis was performed on the raw and neutron-irradiated fibers to determine the thermal behavior of the fibers. DSC analysis also enabled the identification to be made of chemical activity occurring in the fibers as the temperature was increased. The DSC analysis curves of the raw and irradiated jute fibers are shown in Figure 13. A broad endothermic peak observed in the temperature range 60–140°C in both the irradiated and raw jute corresponded to the heat of vaporization of water absorbed in the fibers. It was reported[38] that in cellulose fibers, lignin degrades at a temperature around 200°C, whereas in other polysaccharides such cellulose degrades at a higher temperature. Therefore, these exothermic peaks, which were at temperatures higher than 200°C, indicated the decomposition of cellulose in the fibers. The region between 150 and 240°C showed no exothermic or endothermic reactions, which suggested that the fibers were stable between these temperatures. The first exothermic peak in the DSC curve for the raw jute fiber was at about 290.2°C, which was due to the thermal degradation of hemicelluloses and the glycosidic linkages of cellulose. The very strong second endothermic peak at about 385.5°C indicated the degradation of cellulose, which led to the formation of char. In addition, there was one more step with a peak at

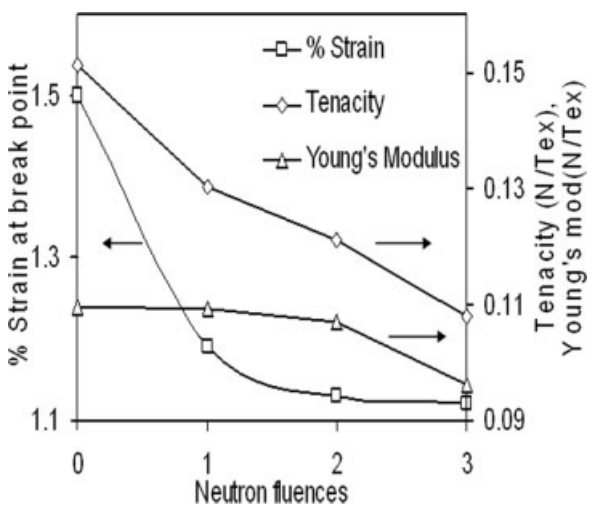

Figure 12 Variation of the strain at break point, tenacity, and modulus of the different jute fibers.

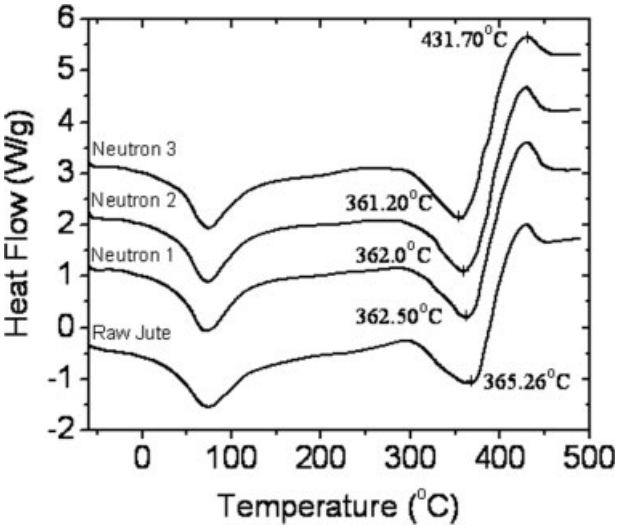

Figure 13 DSC thermograms of the raw and neutron-irradiated jute fibers.

438.7°C. In this step, the rest of the char was oxidized, and the rest of the mass was consumed.[39] From the second endothermic peak, we deduced that the irradiated jute fibers were less thermally stable compared to the raw fibers because the raw fibers had a higher decomposition temperature. It was reported[40] that a decrease in the decomposition temperature may be due to a decrease in the cellulose crystallite size after irradiation, as evidenced by our XRD results.

CONCLUSIONS

The jute fibers (*C. olitorius*) showed the following behavior with neutron fluences of 2×10^{13} n/cm^2 or less:

1. SAXS analysis showed the shrinkage of fiber constituents as the irradiation proceeded.
2. XRD showed a significant compressive stress developed in the fiber, but very small decreases in the crystallite size and CrI were noticed after neutron irradiation.
3. The strength and tensile modulus decreased as the neutron fluences increased.
4. The thermal stability of the fiber decreased after irradiation because of the decrease in the cellulosic crystallite size.
5. Degradation of the fibers due to crosslinking or chain scissoring by fast neutrons was not fully detected by means of FTIR.
6. Fast neutron irradiation showed little effect on the SEM microstructure.

The authors acknowledge S. K. Sarangi (Director of the National Institute of Technology, Rourkela, Orissa, India) for

providing the platform to carry out the research and for constant encouragement. J. Belare (Indian Institute of Technology, Bombay, India) is acknowledged for providing the SAXS facility. N. V. Bhat (Emeritus Professor of Physics, Bombay Textile Research Association) is acknowledged for useful discussion and suggestions for SAXS data analysis. T. N. Tiwari (Retired Professor of Physics, National Institute of Technology) is acknowledged for a thorough reading of the article and valuable suggestions. S. Saha (National Institute of Research on Jute and Allied Fibre Technology (NIRJAFT), Kolkata, India) is also acknowledged for his help during the mechanical testing of the fiber and its property analysis.

References

1. Mohanty, A.; Misra, M.; Hincrichsen, G. Macromol Mater Eng 2000, 1, 276.
2. Felix, J. M.; Gatenholm, P. J Appl Polym Sci 1991, 42, 609.
3. Bisanda, E. T. N.; Ansell, M. P. Composite Science Technology 1981, 41, 165.
4. El-Naggar, M. A.; El-Hosamy, B. M.; Zohdy, H. M.; Zahran, H. A. American Dyestuff Reporter 1992, January, 40.
5. Williams, J. L.; Woods, D. K.; Stannett, V.; Sello, S. B.; Stevens, C. V. Int Journal of Radiat Isotopes 1975, 26, 169.
6. Ranganathan, R. S.; Quayyum, Z. New Horizon for Jute; State-of-Art Report 5; National Information Centre for Textile and Allied Subjects: Ahmedabad, India, 1993.
7. Ishigure, K.; Egusa, S.; Tagawa, S.; Tabata, Y. Radiat Phys Chem 1979, 14, 585.
8. Blazewicz S., Piekarczyk J., Chlopek J., Blocki J., Michalowski J., Stodulski M., Zychowski, P. Carbon 2002, 40, 721.
9. Megusar, J. J Nucl Mater 1996, 228, 168.
10. Spiebberger, S. M. Cryogenics 1997, 37, 135.
11. Krishnamurti, P. Ind J Phys 1930, 5, 473.
12. Mark, H. Physik and Chemie der Zellulose; Springer: Berlin, 1932; p 139.
13. Hendricks, S. B. Z Kristollogr Mine 1930, 74, 534.
14. Porod, G. Kolloid Z 1951, 124, 83.
15. Porod, G. Kolloid Z 1952, 125, 51.
16. Vonk, C. G. J Appl Crystallogr 1973, 6, 81.
17. Roy, S. C. J Text Res 1960, 30, 451.
18. Porod, G. Kolloid Z Z Polym 1953, 133, 16.
19. Ratho, T.; Sahu, N. C. Kolloid, Z Z Polym 1970, 236, 43.
20. Knoll, G. F. Radiation Detection and Measurement; Wiley: New York, 1989; pp 20 and 57.
21. Leo, W. R. Techniques for Nuclear and Particle Physics Experiments; Springer-Verlag: New York, 1987; p 8.
22. Misra, T.; Patra, K. C.; Patel, T. Colloid Polym Sci 1984, 262, 611.
23. Mering, J.; Tchoubar, D. J Appl Crystallogr 1965, 1, 153.
24. Gerber, T.; Walter, G.; Krenold, R. J Appl Crystallogr 1982, 15, 143.
25. Kortleve, G.; Vonk, C. G. Kolloid Z Z Polym 1968, 225, 124.
26. Mittelbach, P.; Porod, G. Kolloid Z Z Polym 1965, 202, 40.
27. Ruland, W. J Appl Crystallogr 1971, 4, 70.
28. Cullity, B. D. Elements of X-Ray Diffraction; Addison-Wesley: London, 1978; p 286.
29. Segal, L.; Creely, J.; Martin, C. Text Res J 1959, 29, 786.
30. Tserki, V. Compos A 2005, 36, 1110.
31. Vonk, C. G. J Appl Crystallogr 1975, 8, 340.
32. Mohlethaler, K. Biochem Biophys Acta 1949, 3, 15.
33. Jones, D. M. Adv Carbohydr Chem 1964, 19, 219.
34. Misra, T.; Bisoyi, D. K.; Patel, T.; Patra, K. C.; Patel, A. Polym J 1988, 20, 739.
35. Khan, M. N. Ph.D. Thesis, Sambalpur University, 1995.
36. Liao, B.; Huang, Y.; Cong, G. J Appl Polym Sci 1997, 66, 1561.
37. Maharana, S.; Tripathy, S. S. J Appl Polym Sci 1991, 42, 1001.
38. Aziz, S. H.; Ansell, M. P. Compos Sci Technol 2004, 64, 1219.
39. Paunikallio, T.; Suvanto, M.; Pakkanen, T. T. J Appl Polym Sci 2004, 91, 2676.
40. Mwaikambo, L. Ph.D. Thesis, University of Bath, 2002.